Feasibility of periodic stabilizers for extending coiled tubing reach

Liljenhjerte, Johannes; Vudayagiri, Sindhu; von Solms, Nicolas; Nygaard, Jens Vinge

Published in:
Geoenergy Science and Engineering

Link to article, DOI:
10.1016/j.geoen.2023.211779

Publication date:
2023

Document Version
Publisher's PDF, also known as Version of record

227 (2023) 211779

Contents lists available at ScienceDirect

Geoenergy Science and Engineering

journal homepage: www.sciencedirect.com/journal/geoenergy-science-and-engineering

Feasibility of periodic stabilizers for extending coiled tubing reach

Johannes Liljenhjerte [a], Sindhu Vudayagiri [b], Nicolas von Solms [b], Jens Vinge Nygaard [a,*]

[a] Department of Biological and Chemical Engineering, Aarhus University, Aarhus 8000, Denmark
[b] Center for Energy Resources Engineering, Department of Chemical and Biochemical Engineering, Technical University of Denmark, Kgs Lyngby 2800, Denmark

ARTICLE INFO

Keywords:
Helical buckling
Increased stability
Periodic support
Tubing force analysis (TFA)
Explicit finite element analysis (FEA)

ABSTRACT

Coiled tubing (CT) operations are widely used to maintain and service wellbores for optimal production. Compressive forces, arising from friction, can cause buckling induced lock-up of the CT, bringing the operation to a halt. This paper investigates the feasibility of using strategically placed periodic supports in the wellbore to increase the buckling stability of the CT. Tubing force analysis (TFA) and finite element analysis (FEA) models from literature are modified and used in conjunction to determine exact locations of the individual supports. For the investigated CT operation this resulted in a total of 2153 periodic supports spanning 7 regions of stabilization covering 1890 m. With a strength and strain wise feasible individual support length of 2 mm, the accumulated collapsed length of supports is 4.3 m. This length scale makes it realistic to bring the periodic supports into the wellbore with the bottom hole assembly during CT operations. Conducted experiments demonstrate how inadequate support causes potential detrimental effects for the operation, however, sufficient periodic support maintains its stabilizing integrity beyond the point of helical buckling.

1. Introduction

Buckling induced lock-up during coiled tubing (CT) operations impedes the maintenance and servicing of deep horizontal sections in extended reach wellbores, resulting in suboptimal production.

Current solutions to combat such lock-ups include pipe tapering, pipe straightening, lubricants, vibratory tools and tractors (Bhalla, 1995; Newman et al., 2014; Qin and Gao, 2016; Livescu and Craig, 2017, 2018).

Liljenhjerte and Nygaard (2021) introduced the notion of stabilizing the CT externally by reducing the radial clearance, r_c, at critical locations in order to postpone buckling and thus lock-up. They also presented a tubing force analysis (TFA) model with accompanying algorithms to investigate the obtainable extended reach from a stabilizing initiative. Their result for *where* and *how much* the investigated wellbore should be stabilized in order to extend reach from about 70% to 100% into the payzone is shown in Fig. 1a.

Liljenhjerte et al. (2021) investigated the stability of periodically supported pipes using finite element analysis (FEA), providing guidelines for the configuration of support periodicity based on system parameters and force exposure. Periodic support configurations are evaluated considering two aspects: (1) the periodic support integrity, η_{ps}, which normalizes the periodic buckling load with the continuous one, along with (2) the indentation resistance, Ω_{ind}, which is a measure of how the pipe resists radially indenting into the space between the periodic supports.

This paper combines the knowledge from the TFA (Liljenhjerte and Nygaard, 2021) and FEA (Liljenhjerte et al., 2021) models to determine exact locations of periodic supports that will provide similar stabilization to continuous support. Both models are slightly modified as described in Section 2.

2. Theory and implementation

The theory and implementation of the TFA and FEA models are described in depth by Liljenhjerte and Nygaard (2021), Liljenhjerte et al. (2021), respectively, thus only aspects relevant to introduced modifications and additions are described here.

Liljenhjerte and Nygaard (2021) introduced the provided stabilization with a *provided stability factor*, Ψ, which scaled the critical buckling load given by Eq. (1) (derived/modified by Paslay and Bogy (1964), Dawson (1984), Chen et al. (1989), He and Kyllingstad (1995)).

$$F_{cr} = \Psi\ 2\beta\sqrt{\frac{F_N EI}{r_c}} \tag{1}$$

Where E and I are young's modulus and second moment of inertia of the CT. r_c is the radial clearance between CT and wellbore (Fig. 1a). F_N is the unbuckled normal contact force, Eq. (2). β is a constant that is 1 for sinusoidal buckling ($F_{cr} \rightarrow F_{crs}$) and disputed between 1.401 and

* Corresponding author.
E-mail address: jvn@bce.au.dk (J.V. Nygaard).

https://doi.org/10.1016/j.geoen.2023.211779
Received 22 November 2022; Received in revised form 17 March 2023; Accepted 31 March 2023
Available online 18 May 2023

Nomenclature

Symbol	Explanation [SI-units]
A	Cross-sectional area of the pipe/rod [m^2]
β	Factor used in calculating F_{cr}
E	Young's modulus [Pa]
η_{ps}	Periodic support integrity
F_c	Axial compressive force [N]
F_{cr}	Critical buckling load [N]
F_{crh}	Helical critical buckling load [N]
F_{crs}	Sinusoidal critical buckling load [N]
F_N	Contact force per unit length between pipe and cylindrical confinement [N/m]
F_{nh}	Contact force per unit length between pipe and cylindrical confinement for a fully formed helix [N/m]
I	Second moment of inertia [m^4]
k_d	Displacement constant/factor
k_τ	Timer period constant/factor
L_{seg}	Length of investigates system [m]
L_{sup}	Longitudinal length of a single support [m]
λ_{crs}	Virtual helical pitch length at F_{crs} [m]
ν	Poisson's ratio
$\bar{O}_{sup}$	Normalized support offset
ω_{cr}	Critical support frequency
Ω_{ind}	Indentation resistance
ω_{sup}	Support frequency
P_{sup}	Support period [m]
r_c	Radial clearance [m]
$r_{c,s}$	r_c in the supported system [m]
R_{con}	Radius of confinement [m]
R_{pip}	Outer radius of rod/pipe [m]
rf	Radial fill fraction
ρ	Density [kg/m^3]
σ_y	Material yield strength [Pa]
T_{pip}	Wall thickness of pipe [m]
T_{sup}	Radial thickness of support [m]
θ_{imp}	Angle imposed on the pipe by F_{imp} [rad]
w	Buoyed pipe weight per unit length [N/m]
ξ_{cm}	Normalized radial indentation between supports

$2\sqrt{2}$ in literature for helical buckling ($F_{cr} \rightarrow F_{crh}$) (Chen et al., 1989; Miska et al., 1996; Mitchell, 1997; Deli et al., 1998).

$$F_N = \sqrt{(w\sin\theta + F_c a_i)^2 + (F_c\ sin\theta\ a_\phi)^2} \tag{2}$$

w is the buoyed weight per unit length, F_c is the compressive force, θ is the inclination angle w.r.t. vertical, a_i is the inclination build rate and a_ϕ is the azimuth build rate.

F_{cr} is a function of F_N, which in turn is a function of $F_c = F_{cr}$ at F_{cr}, thus to obtain the correct F_{crs} and F_{crh} values, an iteration scheme is introduced with Eq. (3). n is the dummy index and it initiates with $F_{cr,n=1} = 0$ and ends when $abs(F_{c,n+1} - F_{c,n})/F_{c,n+1} < 0.0001$.

$$F_{cr,n+1} = \Psi\ 2\beta\sqrt{\frac{\sqrt{(w\sin\theta + F_{cr,n}a_i)^2 + (F_{cr,n}\ sin\theta\ a_\phi)^2}EI}{r_c}} \tag{3}$$

Addition to the TFA model. The virtual helical pitch length, λ_{crs}, at the sinusoidal critical load, F_{crs}, is calculated for each element using Eq. (4).

$$\lambda_{crs} = 2\pi\sqrt{\frac{2EI}{F_{crs}}} \tag{4}$$

λ_{crs} is determined because Liljenhjerte et al. (2021) use it as the characteristic length for which the support frequency, ω_{sup}, is defined as in Eq. (5). Here P_{sup} is the support period indicated in Fig. 1d, and length of interest in order to determine the exact locations of supports.

$$\omega_{sup} = \frac{\lambda_{crs}}{P_{sup}} \rightarrow P_{sup} = \frac{\lambda_{crs}}{\omega_{sup}} \tag{5}$$

For a given ω_{sup}, P_{sup} can be calculated for each element. The minimum P_{sup}, $P_{sup,min}$, for each support cluster of length $L_{cluster}$ is determined and used to calculate their total number of supports.

$$N_{cluster} = ceil(L_{cluster}/P_{sup,min}) + 1 \tag{6}$$

Where ceil is rounding up to rather put one too many support than one to few, and "+ 1" is to go from elements to nodes and to consider that a support should be placed at both ends of the cluster. Each individual support location is then determined using the "linspace" function in MATLAB (2020) and saved in the array $S_{cluster}$.

$$S_{cluster} = linspace(x_s, x_e, N_{cluster}) \tag{7}$$

Where x_s and x_e are the measured depths at the start and end locations of the given cluster, respectively, exemplified in Fig. 1b. The actual P_{sup} for the cluster will be slightly smaller than the $P_{sup,min}$. Doing this for each cluster yields all periodic support locations throughout the wellbore.

Because some gaps between support clusters can be on the scale of P_{sup}, it can be beneficial to combine the clusters by closing the gaps, as illustrated in Fig. 1b. It can also be a good idea to extend the stabilized regions by a few meters in each end for extra safety margins.

Modification to the TFA model. When Ψ is increased by reducing r_c, this reduction should also be considered when calculating the helical buckled contact forces in stabilized regions, F_{nhs}, as indicated in Eq. (8).

$$F_{nh} = \frac{F_c^2 r_c}{4EI} \rightarrow F_{nh,s} = \frac{F_c^2}{4EI}\frac{r_c}{\Psi^2} \tag{8}$$

F_{nh} was derived by Mitchell (1988) and the inclusion of Ψ for $F_{nh,s}$ converts r_c to the supported clearance, $r_{c,s}$, coming from Eq. (9) given by Liljenhjerte and Nygaard (2021), where $rf = 1 - r_{c,s}/r_c$ is the radial fill.

$$\Psi = \sqrt{\frac{r_c}{r_{c,s}}} = \frac{1}{\sqrt{1-rf}} \rightarrow rf = 1 - \Psi^{-2} \tag{9}$$

Modification to the FEA model. Because Liljenhjerte et al. (2021) only investigated straight segments, curvature is introduced into the FEA model to ensure a suitable ω_{sup} can be picked for Eq. (5). An inclination build rate of $a_i = 0.0016$ was chosen, adding about 35% to the average of positive values for the build rate in the regions of being supported ($a_{i,ave+} = 0.00118$). a_ϕ has less influence due to the Pythagorean addition (Eq. (2)) w.r.t. the weight contribution from the CT, thus a_ϕ is set to 0 to keep it simpler.

For the VUAMP subroutines to still properly work with the curvature, the system is translated such that the centerline of the wellbore/supports is at (0, 0) in the xy-plane (Fig. 1c/d) at the point of the applied imperfection force (described in Liljenhjerte et al. (2021)). Since the centerline will not follow exactly the z-direction due to the curvature, there will be a negligible small error in the measured θ_{imp} value.

Gravity is split into a y and z component (Fig. 1c/d) such that it is normal to the centerline at half of L_{seg}, the length of the investigated segment.

The "helical buckling initiation radius" used to identify when buckling initiates set to $0.97 \cdot r_{c,s}$ by Liljenhjerte et al. (2021) is changed to $0.9 \cdot r_{c,s}$ due to the segment curvature. This causes the identified buckling

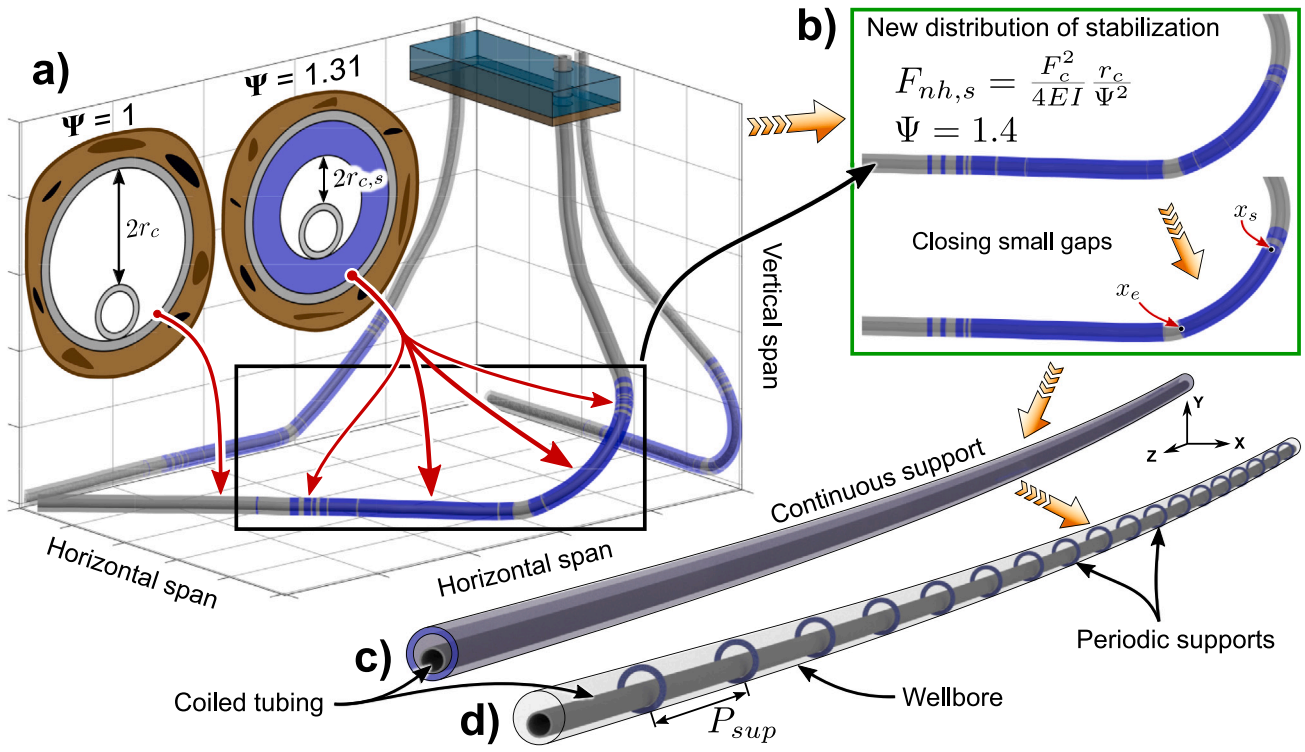

Fig. 1. **(a)** Distributed stabilization found by Liljenhjerte and Nygaard (2021) (total depth of 6.06 km). **(b)** Distribution found after modifications made in this paper, before and after closing small gaps. Contains an example of x_s and x_e for one of the regions (Eq. (7)). **(c)** Continuously supported curved segment with $rf = 0.5$. **(d)** System similar to (c), but periodically supported.

loads to be higher as the compressive forces increase by 5%–10% in the first 0%–10% of the helix formation process as shown by Liljenhjerte et al. (2021). Since it is a comparative study between continuously and periodically supported systems, this overestimate cancels out.

Fixed parameters: $R_{pip} = 25$ mm, $T_{pip} = 4$ mm, $R_{con} = 50$ mm, $L_{seg} = 2.3 \cdot \lambda_{crs}$, $E = 210$ GPa, $\sigma_y = 552$ MPa, $\nu = 0.3$, $\rho = 7800$ kg/m^3, CoF $= 0.28$, $k_\tau = 5$, $k_d = 5$.

Swept parameters: $rf = [0.25, 0.5]$, $\omega_{sup} = [3, 4, 5, 6, 7, 8, 9, 10, 11, 12, 13, 14]$, $\phi_{sup} = [0.001, 0.01]$, $\bar{O}_{sup} = [0, .1, .2, .3, .4, .5, .6, .7, .8, .9]$.

ϕ_{sup} is the fraction of longitudinal length covered by support (L_{sup}/P_{sup}), and $\bar{O}_{sup}$ is the normalized offset from the segment end w.r.t. P_{sup} of all supports in the longitudinal direction. See nomenclature for other parameter descriptions.

3. Experiment

For a proof of concept and to gain mechanical insights of the system, three experimental tests were conducted. One with no supports, one inadequately supported ($\omega_{sup} \approx 4$) and one sufficiently supported ($\omega_{sup} \approx 8$). Material properties were similar to that of the FEA simulations. The setup is straight (no curvature) and is described in the supplementary material, *SI1*.

Geometric parameters: $R_{pip} = 5$ mm, $T_{pip} = 1$ mm, $R_{con} = 11$ mm, $L_{seg} = 6$ m, $L_{sup} = 50$ mm, $T_{sup} = 4.65$ mm ($rf = 0.775$).

4. Data & results

Distribution of stabilization. Fig. 1b shows the new distribution of stabilization after the implemented changes described in Section 2. It has an accumulated span of 1890 m (31.2% of TD) which is a reduction of 265 m compared to the 2155 m (35.57% of TD) accumulated span found by Liljenhjerte and Nygaard (2021). The new distribution has $\Psi = 1.4$ corresponding to a radial fill of 48.98% opposed to the previously $\Psi = 1.31$ ($rf = 41.73$ %). 2 m was added at each end of stabilizing regions before closing gaps of less than 10 m.

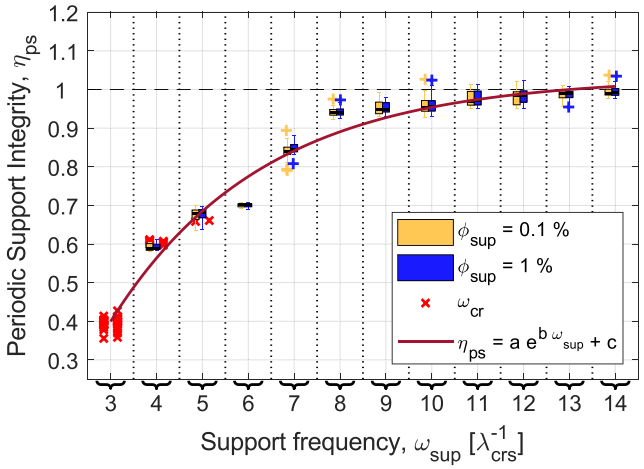

Fig. 2. η_{ps} as a function of the number of supports per λ_{crs} and ϕ_{sup}. rf and $\bar{O}_{sup}$ are grouped in the boxes. It suggests that as $\omega_{sup} \geq 8$, periodic supports are 90%–100% as effective as a continuous one.

Periodic support integrity, η_{ps}. Fig. 2 shows η_{ps} as a function of ω_{sup} and ϕ_{sup} suggesting that periodic supports provide a F_{crh} of 90%–100% of that of a continuous support when $\omega_{sup} \geq 8$. ϕ_{sup} appears to have no significant influence on the system at 0.1%–1%.

An exponential fit over the average values at each ω_{sup} given in Eq. (10) (with $R^2 = 0.9754$) is also added to Fig. 2, as done by Liljenhjerte et al. (2021).

$$\eta_{ps}(\omega_{sup}) = -1.556 \cdot e^{-0.3004\ \omega_{sup}} + 1.031 \tag{10}$$

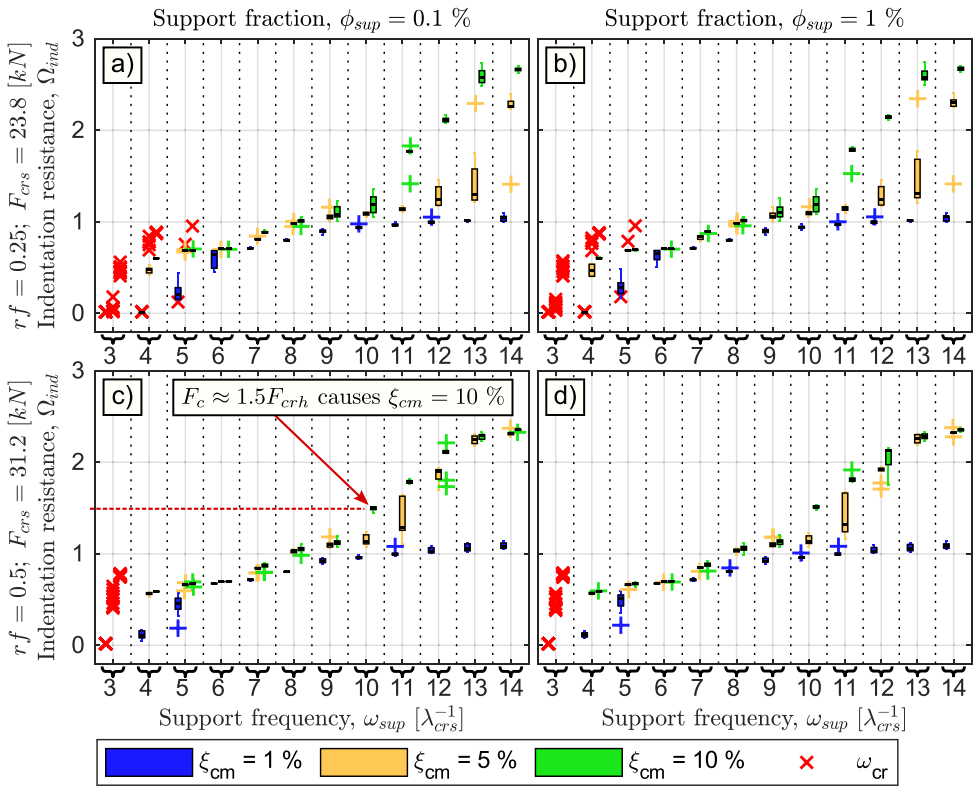

Fig. 3. Indentation resistance, Ω_{ind}, as a function of ω_{sup} for **(a)** $rf = 0.25$ and $\phi_{sup} = 0.1$%, **(b)** $rf = 0.25$ and $\phi_{sup} = 1$%, **(c)** $rf = 0.5$ and $\phi_{sup} = 0.1$%, and **(d)** $rf = 0.5$ and $\phi_{sup} = 1$%. Taking **(c)** with $\omega_{sup} = 10$ and $\xi_{cm} = 10$ % (highlighted), here the $\Omega_{ind} \approx 1.5$, meaning that $F_c \approx 1.5F_{crh}$ (continuous) causes a radial indentation between supports equal to 10% of R_{pip}. Indentation of a given level will happen before helical buckling occurs if $\Omega_{ind} < 1$. **(b)** and **(c)** are comparable to their uncurved counterparts in *fig. 16a1 and a4* in Liljenhjerte et al. (2021), respectively ($rf = 0.25$ is the same as $\rho_c = 0.75$ with the given geometries).

ω_{cr} in Figs. 2 and 3 indicates less reliable data as the buckling identification algorithm is prematurely triggered due to inadequate support.

Indentation resistance, Ω_{ind}. Fig. 3 shows Ω_{ind} as a function of ω_{sup} and ξ_{cm}. The latter being the radial indentation into the gaps between supports as fraction/percentage of the R_{pip}; thus $\xi_{cm} > 2$, means the entire diameter of the pipe is radially located between the supports at the point of most indentation. Fig. 3 suggests that $\omega_{sup} \geq 9$ will suffice for all combinations of rf and ϕ_{sup} investigated if $\xi_{cm} = 5$% is allowed and Ω_{ind} does not have to be higher than 1.

Individual locations for supports. Picking a $\omega_{sup} = 10$, P_{sup} is calculated for each element using Eq. (5) with the λ_{crs} data from the TFA model. $P_{sup,min}$ is found and then $N_{cluster}$ is determined with Eq. (6), where after the individual locations are found with Eq. (7).

This results in a total of 2153 individual supports throughout the wellbore spread out over 7 clusters with an actual P_{sup} varying from 0.82 to 1.083 m between them. With a $\phi_{sup} = 0.1$% this yields a length of the individual supports of 0.82 to 1.083 mm.

New radial fill. The effective stabilization should amount to $\Psi = 1.4$ which result in a $rf = 48.98$% for continuous support. The compromise of Ψ from η_{ps} updates Eq. (9) to Eq. (11) for periodic support.

With $\eta_{ps} = 0.9$ according to Fig. 2 using $\omega_{sup} = 10$ results in a true minimum rf of 58.67% for periodic support.

$$rf = 1 - \left(\Psi/\eta_{ps}\right)^{-2} \tag{11}$$

Experiments. Fig. 4 shows the applied load vs displacement plot of the three tests. $\omega_{sup} = 4$ and 8 have the same near linear load development up until **A**, then $\omega_{sup} = 4$ starts to indent into the gap between periodic supports until it reaches the inner wall of the confinement at **B**. From **B** to **C** it follows the unsupported reference system.

$\omega_{sup} = 8$ goes beyond helical buckling without indenting. This is not what is suggested in Fig. 3 as $\Omega_{ind} \approx 1$ for $\omega_{sup} = 8$ in all cases, however, this is because the experiments are on a straight segment, and not curved as the FEA simulations in this paper. Thus with $\phi_{sup} \approx 13$ % and $\rho_c = 0.27$ *figs. 16a8 (almost same ρ_c) and 17a8 (similar geometric configuration)* in Liljenhjerte et al. (2021) are better benchmarks, having $\Omega_{ind} \approx 1.5$ for $\xi_{cm} = 5$ %.

5. Discussion

Stability integrity and indentation. Segments with curvature require higher ω_{sup} to obtain similar η_{ps} and Ω_{ind} levels documented for straight segments by Liljenhjerte et al. (2021). Ω_{ind} is additionally lowered because the critical loads are larger for curved segments, thus Ω_{ind} is decreased for the same values of F_c, which causes the material yield limit to be reached at lower Ω_{ind}. The material yield limit is observed as the plateau at $\Omega_{ind} \approx 2.4$ for $\xi_{cm} = 5$ and 10% at $\omega_{sup} = 13$ and 14 in Fig. 3c and d. $\eta_{ps}(\omega_{sup})$ in curved segments can still be described with an exponential function.

Choice of $\omega_{sup} = 10$. The choice is based on being slightly higher (more conservative) than the 8 and 9 suggested by Figs. 2 ($\eta_{ps} > 0.9$) and 3c ($\Omega_{ind} > 1$ for $\xi_{cm} \geq 5$%). Fig. 3c was used because it has an $rf = 0.5$ which is closest to the 58.67% found with Eq. (11) and to keep a low ϕ_{sup}, also Fig. 3c differs insignificantly from Fig. 3d.

The TFA model shows an average $F_c/F_{crh} = 0.97$ across the supported regions, meaning that $\Omega_{ind} > 1$ will suffice in most of the total span. However, with a maximum of $F_c/F_{crh} = 1.72$ it is recommended to have a higher ω_{sup} in those regions, or some more indentation may occur, which could be detrimental.

Periodic supports. Increasing the length of the 2153 supports to 2 mm each, would result in an accumulated collapsed length of 4.3 m. Such a length sounds feasible as a canister attached to the typically 10–30 m long bottom hole assembly, that could then drop of the supports

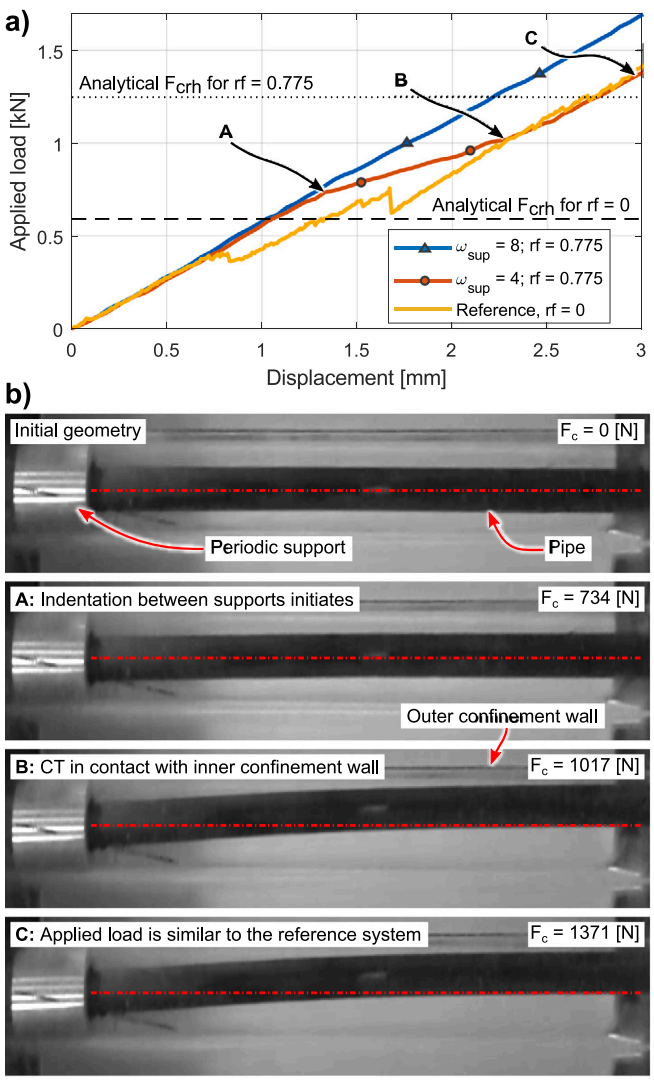

Fig. 4. **(a)** Force vs displacement plot of the unsupported, inadequately supported and sufficiently supported systems along with analytical F_{crh} (Eq. (1) using $\beta = 2$ as Liljenhjerte et al. (2021)). **(b)** Geometric development of the inadequately supported system (distorted to magnify the lateral displacement of the pipe). State **A**, **B** and **C** are indicated in (a).

at the defined locations. From the TFA model, the largest contact forces were about 115 N/m as the CT is injected to total depth. With P_{sup} up to 1.08 m, this yields a normal force of about 125 N that the supports should withstand. Considering a 2 × 2 mm square, such a load would induce a stress of 32 MPa and a strain of less than 0.1% for materials with $E > 32$ GPa. Thus a 2 mm thick steel disk ($L_{sup} = 2$) would have a tremendous safety margin in terms of strength and stiffness.

Note that periodic supports were placed linearly in each cluster based on the $P_{sup,min}$ for the given cluster using a constant ω_{sup}. By considering the individual λ_{crs} and an adaptable ω_{sup} based on forces, optimization algorithms would certainly be able to reduce the number of required supports.

Experiments. Liljenhjerte et al. (2021) reported that as r_c is reduced, the system approaches a linear force response, thus Fig. 4a shows how the $\omega_{sup} = 8$ provides an effective reduction in r_c. $\omega_{sup} = 4$ shows that inadequate support will still increase the linear region (up to **A** in Fig. 4a), but may prematurely transitions to the reference force response (**B** in Fig. 4a), due to indentation (**B** in Fig. 4b), potentially causing detrimental effects for a moving CT. This is of course only the case, if the applied load exceeds that at **A** in Fig. 4a.

6. Conclusion

Results shows that using 2153 strategically placed periodic supports with an rf of 58.67% and a length as low as 1 mm will extend CT reach from 70 to 100% into the payzone.

Using 2 mm thick steel disks as supports ($L_{sup} = 2$) would yield a 4.3 m accumulated collapsed length, which could be stored in a canister on the bottom hole assembly and dropped at the exact locations found with presented methods. 2 mm thick steel disks would be able to carry the maximum contact force found with the TFA model of about 115 N/m.

The number of periodic supports, and thus the 4.3 m collapsed length, could be reduced with future optimization algorithms.

Experiments verify the concept of using periodic supports to change the mechanical response of the system towards a more linear response due to the lower effective radial clearance.

Higher support frequency, ω_{sup}, is required for curved segments in order to obtain similar stability as in the straight system. The periodic stability integrity can still be described as an exponential function of ω_{sup} when including curvature.

Declaration of competing interest

The authors declare that they have no known competing financial interests or personal relationships that could have appeared to influence the work reported in this paper.

Data availability

The authors do not have permission to share data.

Acknowledgments

The authors would like to thank the Danish Hydrocarbon Research and Technology Center (DHRTC) for financially supporting this study.

Additionally, the authors appreciate the efforts of Søren Peder Madsen in maintaining and assisting with optimal usage of the Aarhus University computing cluster "PRIME".

Appendix A. Supplementary data

Supplementary material related to this article can be found online at https://doi.org/10.1016/j.geoen.2023.211779.

References

Bhalla, K., 1995. Coiled tubing extended reach technology. In: SPE Offshore Europe Conference and Exhibition, vol.All Days, http://dx.doi.org/10.2118/30404-MS, SPE-30404-MS.

Chen, V., Lin, V., Cheatham, J., 1989. An analysis of tubing and casing buckling in horizontal wells. In: OTC Offshore Technology Conference, vol.All Days, http://dx.doi.org/10.4043/6037-MS, OTC-6037-MS.

Dawson, R., 1984. Drill pipe buckling in inclined holes. J. Pet. Technol. 36 (10), 1734–1738. http://dx.doi.org/10.2118/11167-PA.

Deli, G., Liu, F., Xu, B., 1998. An analysis of helical buckling of long tubulars in horizontal wells. In: SPE International Oil and Gas Conference and Exhibition in China, vol.All Days, http://dx.doi.org/10.2118/50931-MS, SPE-50931-MS.

He, X., Kyllingstad, A., 1995. Helical buckling and lock-up conditions for coiled tubing in curved wells. SPE Drill. Compl. 10 (01), 10–15. http://dx.doi.org/10.2118/25370-PA.

Liljenhjerte, J., Nygaard, J.V., 2021. Evaluating stabilizing initiatives to extend coiled tubing reach. J. Pet. Sci. Eng. 205, 108905. http://dx.doi.org/10.1016/j.petrol.2021.108905, URL https://www.sciencedirect.com/science/article/pii/S0920410521005660.

Liljenhjerte, J., Vudayagiri, S., von Solms, N., Nygaard, J.V., 2021. Stability of periodically supported slender structures and quantification of Helix formation. Appl. Eng. Sci. 100070. http://dx.doi.org/10.1016/j.apples.2021.100070, URL https://www.sciencedirect.com/science/article/pii/S2666496821000340.

Livescu, S., Craig, S., 2017. A critical review of the coiled tubing friction-reducing technologies in extended-reach wells. Part 1: Lubricants. J. Pet. Sci. Eng. 157, 747–759. http://dx.doi.org/10.1016/j.petrol.2017.07.072, URL https://www.sciencedirect.com/science/article/pii/S0920410517306228.

Livescu, S., Craig, S., 2018. A critical review of the coiled tubing friction-reducing technologies in extended-reach wells. Part 2: Vibratory tools and tractors. J. Pet. Sci. Eng. 166, 44–54. http://dx.doi.org/10.1016/j.petrol.2018.03.026, URL https://www.sciencedirect.com/science/article/pii/S0920410518302134.

MATLAB, 2020. 9.9.0.1495850 (R2020b). The MathWorks Inc., Natick, Massachusetts.

Miska, S., Qiu, W., Volk, L., Cunha, J., 1996. An improved analysis of axial force along coiled tubing in inclined/horizontal wellbores. In: SPE/CIM International Conference on Horizontal Well Technology, vol.All Days, http://dx.doi.org/10.2118/37056-MS, SPE-37056-MS.

Mitchell, R., 1988. New concepts for Helical buckling. SPE Drill. Eng. 3, 303–310. http://dx.doi.org/10.2118/15470-PA.

Mitchell, R., 1997. Effects of well deviation on Helical buckling. SPE Drill. Compl. 12 (01), 63–70. http://dx.doi.org/10.2118/29462-PA.

Newman, K., Kelleher, P., Smalley, E., 2014. CT extended reach: Can we reach farther?. In: SPE/ICoTA Well Intervention Conference and Exhibition, vol.Day 1 Tue, March 25, 2014, http://dx.doi.org/10.2118/168235-MS, D011S001R004.

Paslay, P.R., Bogy, D.B., 1964. The stability of a circular rod laterally constrained to be in contact with an inclined circular cylinder. J. Appl. Mech. 31 (4), 605–610. http://dx.doi.org/10.1115/1.3629721.

Qin, X., Gao, D., 2016. The effect of residual bending on coiled tubing buckling behavior in a horizontal well. J. Nat. Gas Sci. Eng. 30, 182–194. http://dx.doi.org/10.1016/j.jngse.2016.02.016, URL https://www.sciencedirect.com/science/article/pii/S1875510016300622.